Sea level rise inducing tidal modulation along the coasts of Bengal delta

Md Jamal Uddin Khan [a,*], Fabien Durand [a,b], Laurent Testut [a,c], Yann Krien [c], A.K. M. Saiful Islam [d]

[a] LEGOS UMR5566, CNRS/CNES/IRD/UPS, 31400, Toulouse, France
[b] Laboratório de Geoquímica, Instituto de Geociencias, Universidade de Brasilia, Brazil
[c] LIENSs UMR 7266 CNRS, La Rochelle University, 17000, La Rochelle, France
[d] IWFM, BUET, Dhaka, 1000, Bangladesh

ARTICLE INFO

ABSTRACT

The Bengal delta, the largest delta on the Earth, is subject to a marked coastal flooding hazard and associated with widespread vulnerability. The situation will expectedly deteriorate in the ongoing context of sea level rise. This sea level rise will not only have a direct effect on the coastal flooding, but will also have indirect effects, through the alteration of the coastal hydrodynamics. In the present study, we investigate the impact of sea level rise on tide, which is the largest source of variability of sea level along the macro-tidal coast of Bengal delta. Through a comprehensive modelling framework comprising the coastal delta, major estuaries, as well as the intricate hydraulic network of the delta, we assess the future changes of tidal properties to be expected for various sea level rise scenarios, representative of the end of the 21st century and beyond. It is found that the effect is large, and regionally dependent. Over both the south-western and south-eastern parts of the delta, the amplitude of the tide is expected to increase when the sea level is higher, which is bound to aggravate the tidal flooding hazard. In contrast, the central part of the delta will potentially experience massive flooding of river banks and adjoining lands in the scenarios exceeding 0.5 m of sea level rise. Consequently, this flooding induces a decay of the tidal amplitude in the central part. Our study shows that the tidal modulation is a significant ingredient that needs to be accounted for in the evolution of the future hydrodynamics of the Bengal delta. The friction-dominated and regionally contrasting damping and amplification mechanism also underscores the potential application of managed realignment strategy for a sustainable delta management in the future.

1. Introduction

Based on tide-gauge records, the global sea level has risen at a rate of about 1.1 mm/year on average over the 20th century (Dangendorf et al., 2017). The advent of altimetry revealed a marked acceleration over the last decades, with a sea level rise reaching 3.58 mm/year over the 2006–2015 period (Oppenheimer et al., 2019). According to IPCC, the projected median sea level rise (SLR) to be expected in 2100 ranges from 0.43 m (0.29–0.59 m, likely range; RCP2.6) to 0.84 m (0.61–1.10 m likely range; RCP8.5) above pre-industrial level (Oppenheimer et al., 2019). Recently, several studies projected even more extreme scenarios, suggesting that an increase of order 2 m should be considered as plausible (e.g. Sweet et al., 2017; Bamber et al., 2019; De Dominicis et al., 2020). Moreover, SLR is *virtually certain* to continue beyond 2100 with an estimated rise of 1–3 m for each 1° temperature increase (Church

et al., 2013). These numbers are alarming, as the coastal population settled in low-lying areas will exceed 1 billion by 2060 (Neumann et al., 2015).

SLR is of even greater concern for the low-lying subsiding delta areas (Tessler et al., 2015; Oppenheimer et al., 2019; Becker et al., 2020). The Ganges-Brahmaputra-Meghna (GBM) delta is a characteristic example of such subsiding deltas for which coastal flooding can be greatly enhanced by SLR (Becker et al., 2020). It is located at the northern head of the Bay of Bengal, covering an area larger than 100,000 km^2 (Fig. 1). The region is densely populated and the delta area sustains more than 150 M people. The typical topography is less than 3 m above mean sea level (Krien et al., 2016) and contains a dense network of rivers and channels. The delta is macrotidal, with a typical tidal range in excess of 4 m (Krien et al. 2016, 2017a; Tazkia et al., 2017). The climate is dominated by the Indian monsoon. During each summer monsoon season, about 1 GT of
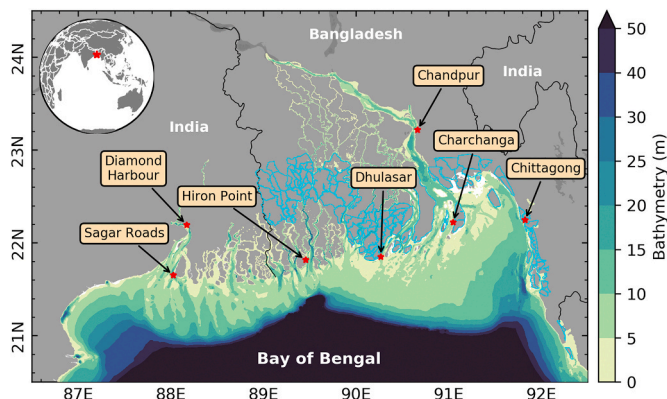
Fig. 1. Layout of the Bengal delta with country borders. The near-shore bathymetry is mapped associated with the color scale. The cyan lines show the limits of the existing polders. The red stars indicate the location of the main tide gauges stations. (For interpretation of the references to color in this figure legend, the reader is referred to the Web version of this article.)

sediment gets flushed through the river network (Goodbred and Kuehl 1999), although in recent years a decreasing trend was reported by Rahman et al. (2018). In this sediment-laden fertile area, agriculture is the dominant land-use. To promote agriculture and manage the saline water intrusions, 126 polders (i.e. low-lying areas surrounded by embankments) were built during the period 1960 to 1990 (World Bank 2005). These polders occupy the southern-central part of the delta (Fig. 1). These polders, however, restrict sediment distribution over land and infilling of tidal channels (Auerbach et al., 2015). While the regional estimate of the subsidence ranges from 1 to 7 mm/year (Krien et al., 2019; Becker et al., 2020), Auerbach et al. (2015) report land subsidence as high as 20 mm/year within some polders. This implies that the relative SLR poses a major threat for the ongoing century. In contrast, over the natural part of the GBM delta in the south-central region, the siltation may be able to cope with the effect of SLR (Bomer et al., 2020).

As the tidal sea level is a prominent ingredient of coastal flooding over the GBM delta (Krien et al. 2016, 2017a), the long-term evolution of the tide deserves specific attention. The objective of the present study is to analyse the long-term evolution of the tide expected in the Bengal delta, as a response to SLR. Indeed, tidal characteristics such as tidal range and tidal phase are known to respond to change in mean sea level (MSL), with strongest impacts in the near-shore ocean (Haigh et al., 2019; Talke and Jay 2020). From a quasi-global tide-gauge data archive, Woodworth (2010) reported significant changes of tidal range in several areas and suggested that the changes are probably already occuring globally. The imprint of SLR on tidal characteristics is largely dependent on the region considered, amplifying tidal range in some locations, and reducing the tidal range in others (Idier et al. 2017, 2019). This is explained by the various mechanisms through which the mean sea level can affect the propagation of the tidal waves, in particular the frictional and non-frictional processes (Haigh et al., 2019; Talke and Jay 2020). Pickering et al. (2017) produced a global modelling of the projected tidal range under various SLR scenarios, ranging from +0.5 m to +10 m above current level. Over the northern Bay of Bengal, they suggested that a +2 m SLR would induce a contrasted change, with an increase of the tidal range in the eastern part of the GBM coastline, and a decrease in its central-western part. As the modelling initiative of Pickering et al. (2017) was global, it could not represent the details of the geometry of the GBM delta nor its intricate river network. From a limited set of observational sea level records located along the GBM delta shoreline, Pethick and Orford (2013) concluded that the tidal range has been increasing in the central part of the delta in the recent decades, at rates of order 5–30 mm/y, which lies well above the trends of eustatic sea level rise. Hence it is important to investigate this process regionally, in the current context of SLR and associated increased exposure of the

coastal areas to the flooding hazard.

The regional dependency of the impact of SLR on tidal characteristics, combined with the dearth of reliable, long-enough tidal records over the Bengal delta, naturally calls for numerical modelling as an appropriate means to investigate the future evolution of tide over this area. The aim of the present study is to draw firm conclusions on the impact of sea level rise on tides using a regional, high-resolution tidal model of the GBM delta.

In Section 2, we present the observational dataset and long-term trend of the tidal range observed in the central part of the GBM delta. Section 3 features our numerical tidal model and its performance analysis. Section 4 presents the projected changes modelled under the various scenarios we simulated. We present the analysis of our results in Section 5 and we conclude our study in Section 6.

2. Observed trend in tidal range: the example of Hiron Point

In order to illustrate the current trends over the GBM, we will present the signal observed at Hiron Point (89.47°E, 21.78°N, see Fig. 1), in the south-central delta. As pointed out by Pethick and Orford (2013), a major hurdle in the GBM delta is the lack of long, consistent in situ tidal records. Although Hiron Point station stands out as the best documented over the GBM, these authors could only analyse 20 years of hourly records there. Here we analyse an updated, enhanced version of Hiron Point record. The Hiron Point tide gauge is situated in a relatively undisturbed region and maintained by Mongla Port Authority. The tide-gauge dataset is maintained and distributed by the Bangladesh Inland Water Transport Authority. Our timeseries is 40 years long (1977-2017), with few missing years in 2004–2005, 2011–2012, 2014–2016. We computed the daily (25 h) low-water level, daily high-water level and daily tidal range from the hourly water level observations. We then computed monthly (28 days) averages of these quantities to remove the spring-neap cycle. As suggested by Woodworth (2012) we refrained from computing and removing the nodal tide from our timeseries.

Fig. 2 shows the long-term changes and evolution of tidal characteristics in the record of Hiron Point tide gauge. We recall that, being restricted to one unique station, and keeping in mind the regional dependency of the long-term trends of tidal characteristics evidenced by Pickering et al. (2017) along the GBM coastline, this analysis should be considered as a qualitative illustration of the currently observed changes. It may certainly not be considered as representative of the long-term change of tidal characteristics over the whole GBM delta. What is more, Hiron Point tide gauge is located in a narrow creek, and its vertical land motions have not been monitored.

We have calculated the monotonic trend in various quantities of our timeseries using Sen slope (Sen 1968). The significance of our trend is estimated using the Mann-Kendall trend test (Mann 1945; Kendall 1975). As shown by Tazkia et al. (2017), there exists a strong seasonality of the tidal range along the Bengal shoreline. This seasonality is a response to the seasonal cycle of the Bay of Bengal sea level, which is itself a manifestation of the monsoonal forcing of the thermohaline stratification of the Bay of Bengal (Shankar et al., 1996; McCreary et al., 1996; Benshila et al., 2014). We have applied the technique proposed by Hirsch et al. (1982) to test the significance of our trend for a seasonally varying timeseries. Similarly, the amplitude of the trend is calculated using the modified method suggested by Hipel and McLeod (1994).

From our monthly (28-day) average mean sea level, we found that the relative MSL has increased by 4.2 mm/year. This value, although based on the sole, long enough pointwise in situ record we could access, appears representative of the magnitude of SLR observed from spaceborne altimetry over the Northern periphery of the Bay of Bengal during the past three decades (Not shown here, see https://www.aviso.altimetry.fr/es/data/products/ocean-indicators-products/mean-sea-level.html).
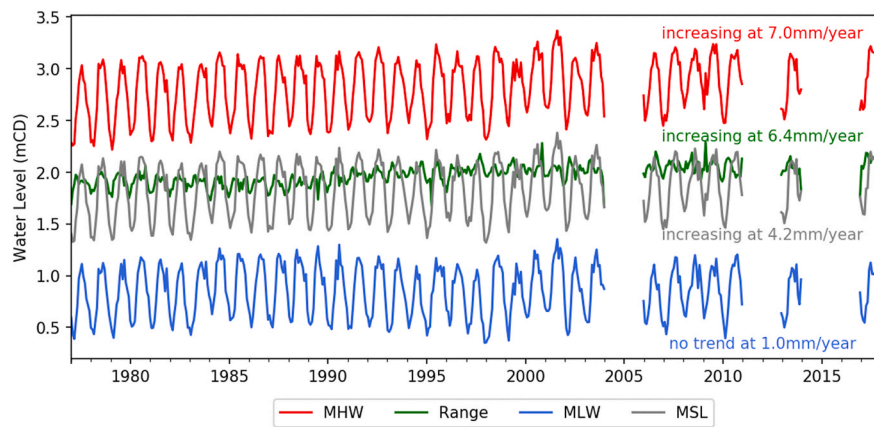
Similar to the MSL, a daily (25 h) maximum and minimum is

Fig. 2. Monthly-mean (28-days) timeseries of observed water level at Hiron Point tide gauge. The red curve shows the mean high water (MHW), the blue curve shows the mean low water (MLW), the green curve shows the mean tidal range (Range), the grey curve shows the mean sea level (MSL). The levels are in meters relative to chart datum (mCD). (For interpretation of the references to color in this figure legend, the reader is referred to the Web version of this article.)

calculated, and then averaged over a month (28 days) to derive the monthly mean high water (MHW) and mean low water (MLW) timeseries. We have found that the MLW has increased at a much lower rate, at 1.0 mm/year, which is statistically not significant at 95% confidence interval and reported here as "no trend". In contrast, the MHW has increased at a much faster rate, 7.0 mm/year. As a result, the tidal range has also increased by 6.4 mm/year. Except the MLW, all other quantities are significant at 95% confidence interval.

These trend estimates essentially confirm and strengthen the findings of Pethick and Orford (2013), that the tidal range in Hiron Point is rising, probably in association with the significant sea level rise observed in the northern Bay of Bengal. The rate we report for the increase in MHW is around twice as large as the one for the MSL. This implies that the long-term changes in tidal characteristics can be a prominent ingredient in the evolution of the flooding hazard in the GBM, in addition to the long-term SLR. Hence the understanding of the underlying processes deserves careful consideration. As there does not exist any other consistent long in situ tidal record over the region, with duration sufficient to address the long-term trends, we hereafter restrict our analysis to numerical modelling, to gain insight on the future evolution of the tidal characteristics at the scale of the whole GBM delta.

3. Tidal model in the Bay of Bengal

The numerical model used in this study, SCHISM (Semi-implicit Cross-scale Hydroscience Integrated System Model, Zhang et al., 2016), is a derivative code of SELFE (Semi-implicit Eulerian-Lagrangian Finite Element) model, originally developed by Zhang and Baptista (2008). It solves the 3D shallow-water equations using finite-element and finite-volume schemes, and was designed to model barotropic as well as baroclinic circulation for a broad range of spatial scales, spanning from the open ocean (e.g. Krien et al., 2016) to the very shallow lagoons and estuaries (e.g. Bertin et al., 2014). The model allows for wetting and drying. Our model set-up and the numerical grid are similar to the version used by Krien et al. (2016) and Tazkia et al. (2017), who investigated the tidal characteristics over the GBM delta and their seasonal variability, respectively. In the present study, however, the domain extends throughout the Bay of Bengal, with a southern boundary located along 11°N (Fig. 3a).

SCHISM is used here in depth-averaged barotropic mode. Our bathymetry is developed over the one published by Krien et al. (2016). Their bathymetry is composed of soundings digitized from navigational charts published by Bangladesh Navy over the near-shore zone, digitized soundings from Inland Waterways Authority of India (IWAI), a high-resolution (50 m) inland topography of the south-central part of the delta from the Center for Environmental and Geographic
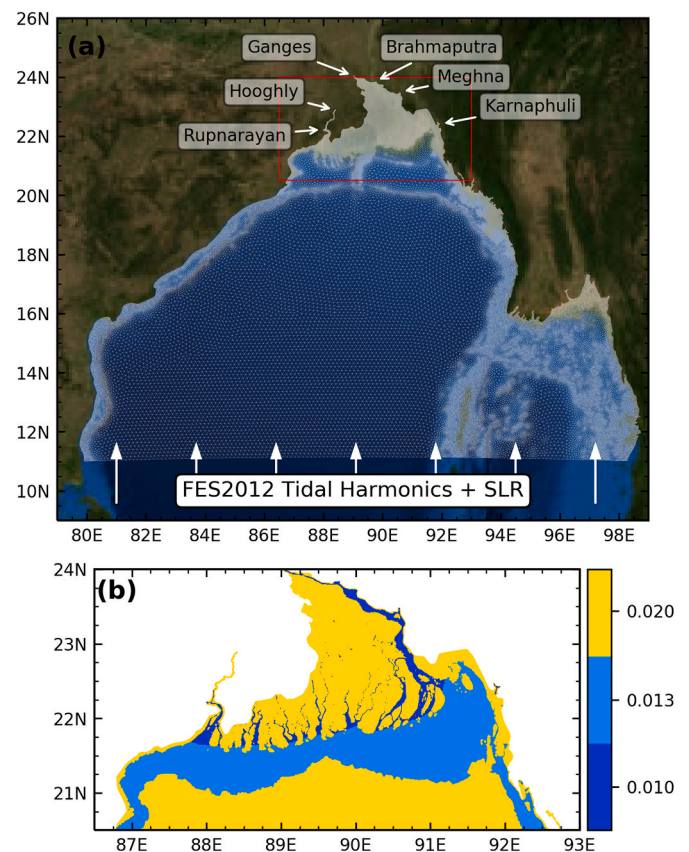

Fig. 3. (a) Model mesh over the computational domain with indication of the open boundary conditions used. Red box indicates close-up area of frame (b). (b) Spatial distribution of the Manning coefficient n (in s.m$^{-1/3}$) used in the model. (For interpretation of the references to color in this figure legend, the reader is referred to the Web version of this article.)

Information Services (CEGIS), and cross-sectional data of the inland rivers from Bangladesh Water Development Board (BWDB). The bathymetry used in this study was updated with digitization of about 77′000 additional points collected from a set of 34 recent nautical charts of the Bangladesh Navy (http://bnhoc.navy.mil.bd/?page_id=165) scattered around the model domain. In the deeper part of the ocean and over the rest of the inland areas we complemented our dataset with GEBCO2014 (https://www.gebco.net/data_and_products/gridded_bath

ymetry_data/) and SRTM (https://www2.jpl.nasa.gov/srtm/cbandda taproducts.html) digital elevation model (as appear in GEBCO dataset) respectively. The grid resolution varies from 15 km in the central Bay of Bengal to 250 m in the most upstream part of the estuaries, which results in about 600′000 nodes and 1 M elements in total.

The bottom friction in our model is formulated through a regionally-varying Manning coefficient n. The spatial distribution of Manning coefficient is similar to Krien at al. (2016) with n = 0.02 for the deep ocean (depth≥20 m) and n = 0.013 over the continental shelf (depth < 20 m). Manning value of 0.01 is set for the rivers, and 0.02 for inland areas (Fig. 3b).

The simulations used in the present study were carried out over a 14-month period, from 01/12/2009 to 31/01/2011. We discarded the first 15 days to let the model flow being spun up, and analysed the subsequent period for tidal analysis. A time-varying discharge was imposed for the Ganges and Brahmaputra rivers (Fig. 3), using observations of the Bangladesh Water Development Board. We have imposed a monthly climatology of discharge for Hooghly river (Mukhopadhyay et al., 2006) and Karnaphuli river (Chowdhury and Al Rahim 2012). At the upstream limit of Meghna and Rupnarayan rivers, a radiative open boundary was prescribed (Flather 1987). Tidal elevations from FES2012 global model (Carrère et al., 2013) were prescribed at the southern open ocean boundary from the global model for the 26 dominant harmonic constituents (M2, M3, M4, M6, M8, Mf, Mm, MN4, Msf, MU2, N2, NU2, O1,

P1, Q1, R2, S1, S2, S4, SSA, T2, K2, K1, J1, and 2N2). As regards to the tidal boundary conditions, the same modelling strategy was followed both for the current-epoch simulations and for the future-scenarios simulations.

The future scenarios are simply defined by superimposing an offset on the model MSL as regards to the current-epoch. Our choice of forcing the model at its southern open boundary with a present-day tidal solution was motivated by the findings of Pickering et al. (2017), who concluded that in the future SLR scenarios, the tidal amplitude remains practically unchanged in the southern part of the Bay of Bengal. This forcing strategy will be validated in Section 4, where we will conclude to a good consistency of our modelled changes and the one reported by Pickering et al. (2017) throughout the coastal part of the northern Bay of Bengal.

As we have significantly upgraded the bathymetry of our model compared to the past studies conducted with it, it is important to assess the realism of the tide simulated. The tidal analysis of the model outputs was achieved through the COMODO software (Allain 2016). Table 1 presents the model performance, expressed in terms of amplitude, phase and complex error of the four dominant tidal constituents (M2, S2, K1 and O1) against observed values. Wherever possible, we also present our model performance against four state-of-the-art global tidal atlases, as follows:

Table 1

Amplitudes (A) and errors (σ_s) are in centimetres, phases (Φ) is in degrees. Because of their location far upstream in the estuaries, Diamond Harbour and Chandpur, are not represented in global tidal models (FES, GOT, and TPXO).

Station		Observation			FES2012-Hydro			FES2012			GOT4.8			TPXO7.2			Krien2016			Current model		
		A_0	Φ_0		A_m	Φ_m	Error	A_m	Φ_m	Error	A_m	Φ_m	Error	A_m	Φ_m	Error	A_m	Φ_m	Error	A_m	Φ_m	Error
Sagar Roads (88.0300°E, 21.6500°N)	M2	140	116		142	99	42	137	104	29	113	113	27	132	104	28	143	116	3	144	115	5
	S2	66	150		73	141	13	62	141	11	40	145	40	48	126	29	62	155	7	62	153	5
	K1	15	262		17	256	2	16	253	3	14	277	14	14	258	1	17	265	2	16	265	1
	O1	5	250		6	251	1	6	243	1	5	270	2	5	252	0.4	6	248	1	6	252	1
	σ_s						31			22			27			29			6			5
Diamond Harbour (88.1733°E, 22.1928°N)	M2	157	168														166	161	21	142	166	16
	S2	68	210														68	207	4	58	209	10
	K1	15	285														16	284	1	13	286	2
	O1	7	258														5	253	2	5	258	2
	σ_s																		15			14
Hiron Point (89.4780°E, 21.8169°N)	M2	81	127		86	88	56	87	91	52	80	88	53	104	110	35	81	115	17	100	115	27
	S2	34	159		45	121	28	40	122	24	37	118	25	37	136	14	35	148	7	42	151	9
	K1	13	268		15	250	5	16	252	5	14	248	5	14	261	2	15	265	2	15	266	2
	O1	5	258		6	244	2	6	238	2	5	244	1	5	256	0.3	6	245	1	6	255	1
	σ_s						44			40			42			27			13			20
Dhulasar (90.2700°E, 21.8500°N)	M2	73	158		68	114	52	80	117	53	79	117	54	86	121	51	51	156	22	68	143	19
	S2	35	193		39	141	33	39	142	32	39	146	29	35	135	34	20	194	15	29	180	10
	K1	13	286		15	262	6	16	256	8	15	260	6	15	255	8	12	297	3	13	288	1
	O1	4	278		6	256	3	6	243	3	6	256	3	6	250	3	5	280	1	6	274	2
	σ_s						44			44			44			44			19			15
Charchanga (91.0500°E, 22.2188°N)	M2	96	234		110	202	57	115	208	50	97	204	49	84	164	103	67	208	46	96	217	28
	S2	37.5	265		38	238	18	30	243	15	34	234	19	36	186	47	27	241	17	37	250	9
	K1	13	304		17	298	4	16	300	4	7	314	6	16	272	8	14	309	2	17	309	4
	O1	8	285		7	289	1	6	284	2	4	303	4	6	267	3	8	289	0	8	293	1
	σ_s						43			37			37			80			35			21
Chittagong (91.8274°E, 22.2434°N)	M2	173	196		118	193	56	126	200	49	120	192	54	89	153	123	156	198	18	149	195	24
	S2	64	229		41	230	23	33	236	31	43	227	21	40	160	62	58	235	9	55	226	10
	K1	19	278		17	294	6	17	295	6	9	300	11	16	258	7	20	289	4	19	285	2
	O1	8	263		7	285	3	6	280	3	4	289	5	6	252	2	8	269	1	8	267	1
	σ_s						43			41			42			98			14			18
Chandpur (90.6385°E, 23.2344°N)	M2	30	31																	34	334	31
	S2	11	62																	11	6	10
	K1	6	29																	5	22	1
	O1	3	13																	4	357	1
	σ_s																					23

- FES2012, the finite-element model (Carrère et al., 2013) built upon altimetry-derived harmonic constant assimilation;
- FES2012-Hydro, the hydrodynamic version of FES2012 (without data assimilation);
- GOT4.8 (Ray 1999, 2013) and TPXO7.2 (Egbert and Erofeeva 2002), two inverse tidal models derived from satellite altimeter data.

We found that, in line with Krien et al. (2016), the tide simulated by our model is far more realistic than the tide of any of the global atlases available. The benefit in terms of mean complex error amounts to an improvement by a factor of 2–6, typically. This can largely be explained by our refined resolution and improved regional bathymetry. Moreover, our new model outperforms the representation of the tide compared to our previous study by Krien et al. (2016), by 10–50% typically, depending on the station considered. The residual errors we obtain range from 5 cm to 23 cm, for the coastal stations as well as for the estuarine stations located further upstream in the GBM delta. This level of realism is unprecedented over our area. Given that we use a similar numerical setup as Krien et al. (2016), with an identical forcing strategy, similar mesh resolution and identical bottom friction coefficient, this means that our improved bathymetry has a prominent impact on the quality of the simulated tide. One exception concerns the Chittagong station, where our model, although far more realistic than the global atlases, does not perform better than the previous version. This could be due to the inclusion of an open boundary in the estuary instead of a closed boundary as in Krien et al. (2016).

4. Projected changes in tidal range in the Bengal delta

4.1. Current tidal range

The mean daily tidal range over 2010 simulated by our model over the GBM delta is shown in Fig. 4a. As expected, it is consistent with the known patterns (Sindhu and Unnikrishnan 2013; Krien et al., 2016; Tazkia et al., 2017). Two maxima of the tidal range are seen in the western part of the delta (Hooghly estuary) and in the eastern part
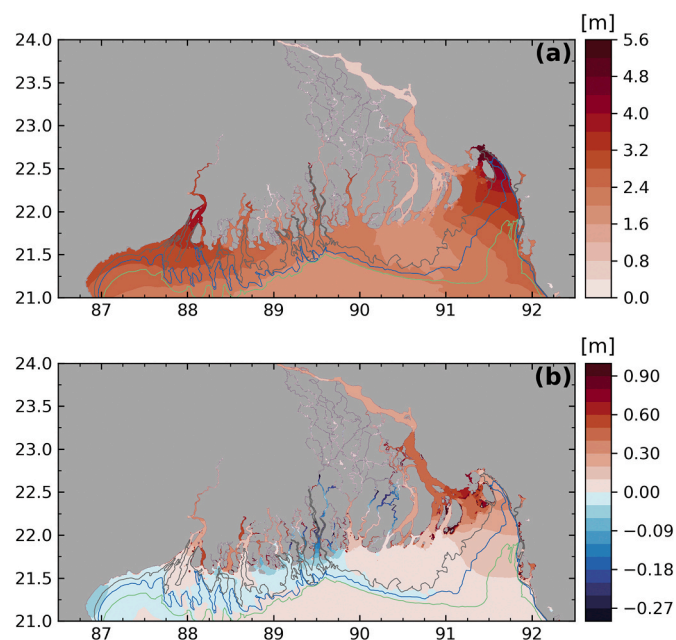
Fig. 4. (a) Mean tidal range for the reference simulation, corresponding to present-day conditions. Isobaths 7 m, 10 m and 15 m are displayed. (b) Difference between the mean tidal range in the +1 m SLR scenario and the reference simulation.

(mouth of Meghna estuary and the north-eastern corner of the Bay of Bengal), with mean tidal ranges reaching 3.2 m and 4.8 m, respectively. In the central part of the coastal GBM from 89°E to 91°E, the mean tidal range is smaller, with values inferior to 2.4 m. On account of the flatness of the delta topography, the tide is seen to propagate far upstream in the various estuaries, beyond 100 km inside Hooghly estuary and inside the various branches of the central delta, and beyond 250 km in the GBM main stream.

4.2. +1 m SLR

Various approaches have been adopted in the past to model the effect of future SLR on the coastal ocean. Some have assumed an unchanged topography (e.g. Krien et al., 2017b; Rahman et al., 2019). In this case, whatever continental areas along the coastal strip currently lying below the elevation of imposed SLR plus the tidal amplitude will get flooded. Opposed to this approach, other studies have assumed that the coastline will remain unchanged under SLR scenarios. Numerically, unchanged coastline under SLR scenarios amounts to assuming that high enough structures protecting the shoreline are implemented consistently everywhere in the model domain, along the current coastline (as done for instance in De Dominicis et al., 2020). A wide range of intermediate, more refined scenarios can be thought of, so as to take into account the spatial structure of vertical land motions (Pickering et al., 2017), the regionally-dependent erosion/accretion pattern of sedimentary plains (Auerbach et al., 2015; Bomer et al., 2020), or regionally-dependent coastal defence enhancement strategies (Feng et al., 2019). Pickering et al. (2017) evidenced a sensible impact of the approach selected among these, on the long-term evolution of tidal characteristics, in some areas of the world ocean (including in the deep ocean). In the absence of definite knowledge of the future evolution of coastal defences in the GBM, nor of the regional pattern of vertical land motion expected to take place over the GBM, and for the sake of simplicity, we assumed an unchanged topography in the present study. In this sense, our coastline can be seen as a soft shoreline: the low-lying coastal areas are freely inundated when the sea level rises. This choice is, we believe, the most reasonable one can make over our region.

In our first future-scenario numerical simulation, we impose a 1 m SLR by imposing a Z0 tidal constituent of null frequency and 1 m amplitude, along the southern open boundary. Numerically, this is equivalent to offsetting downward the model topography/bathymetry by 1 m. We then run the model in the same fashion as in the reference simulation, starting it on 1/12/2009, spinning it up during 15 days, and retaining the subsequent 13.5 months period for analysis. Fig. 4b illustrates the change in mean daily tidal range calculated over one-year period simulated by the model in this +1 m SLR scenario, as compared to the reference simulation. It is seen that the effect is sensible over the whole delta, with contrasted values. In both the western and eastern parts of the coastal GBM, from 87.8°E to 88.8°E, and from 89.8°E to 92°E, the coastal mean tidal range increases, by values of order 10–30 cm. This increase extends upstream in the estuaries outflowing in these two regions, with a particularly enhanced increase in some of them (for instance up to 40 cm in the Hooghly and up to 70 cm at the mouth of Meghna). In contrast, the central part of the delta, from 88.8°E to 89.8°E, exhibits a decrease of the mean tidal range, with values between -3cm and -6cm along the coastline, and stronger values, up to −30cm, in the upstream part of the estuaries.

To gain further understanding on the modelled changes, we analysed separately the change in tidal amplitude for the two main tidal constituents over the GBM, M2 and S2. This was done by subjecting the 13.5 months of model outputs to the same harmonic analysis, both for the reference simulation and for the +1 m SLR experiment, through COMODO software. The results are displayed on Fig. 5.

In our reference simulation, M2 and S2 amplitude pattern is in agreement to past studies, showing two local maxima on the east- and the west-corner with a central trough (Sindhu and Unnikrishnan 2013;

see their Figure 15 for M2 and Figure 10 for S2). We observe a stronger gradient in amplitude compared to theirs with ranges of spatial scale. It is expected given the high resolution of our model, as well as the inclusion of estuaries.

From Fig. 5, It is seen that both tidal constituents contribute to the observed change in tidal range in the +1 m SLR scenario, with a decrease of tidal amplitude along the coastal part of the delta between 88.8°E and 89.8°E. The decrease remains weak along the open coastline (less than 5 cm or 5% for M2, less than 2 cm or 5% for S2) but it extends upstream in the estuaries for both constituents. Both to the west as well as to the east of this central region, the model shows an increase of both M2 and S2 amplitudes along the coastline. In the western part, at the mouth of Hooghly, the increase amounts to 5 cm (5%) for M2 and 2 cm (5%) for S2, and is enhanced northward inside the Hooghly estuary, to about 22.5°N, 100 km upstream of the mouth, for both constituents. In the eastern part of the coastal delta, the increase in tidal amplitude rises eastward, up to extreme values of 15–20 cm (15–20%) at the mouth of Meghna for M2. Similarly, the increase in S2 amplitude also increases eastward, up to values of 10 cm (20%) at the mouth of Meghna. This increase extends northward in the Meghna estuary, and remains in excess of 20 cm for M2 and in excess of 6 cm for S2 up to the bottleneck of Chandpur (23.2°N, 90.6°E).

If we closely look at the central part of the delta shoreline, between 89°E and 90.5°E, what is striking is the contrasted impact of SLR to the west of 89.8°E vs. to the east of 89.8°E, with a decrease of tidal amplitude to the west of this longitude, and an increase to the east of it. However, the tidal range in the reference simulation is fairly homogeneous across this central region. Similarly, the cross-shore variation of bathymetry appears alike, as both sides of this central region sit in the area of narrow submarine delta, with a 15 m isobath located typically not more than 50 km offshore. In this regard, keeping in mind that the delta is both low-lying and very flat in this south-central region, it is relevant to examine the effect of the 1 m SLR on the extent of tidal

flooding. Fig. 6 presents the spatial structure of the frequency of wetting in the current conditions as well as in the +1 m SLR scenario. It is seen that under the +1 m SLR scenario a large fraction of the central delta gets submerged more than 75% of the time, whereas the tidal flooding is minor in the reference conditions. The tidal flooding is widespread in particular in the coastal belt located between 89°E and 89.8°E, where the tidal range is seen to decrease under this SLR scenario. The tidal flooding extends far inland there, up to the edge of the model grid, 75 km upstream or so. A prominent tidal flooding also appears in the inner part of the delta, between 90°E and 90.6°E, to the north of 22.4°N, up to 23°N. To the south of this region, and over the rest of the coastal delta, the currently dry land remains essentially dry in the +1 m SLR scenario, thanks to the embankments present there (Fig. 1).

4.3. Robustness of the projected changes under other SLR scenarios

As the projected SLR by the end of the 21st century has a large uncertainty bound, it is important to get an idea of the linearity of the response of tidal amplitude change to SLR. Beyond the issue of regional dependency of the sign of the expected change in tidal range (positive vs negative) presented in section 4.2, the past modelling studies of Pickering et al. (2017) and Feng et al. (2019) concluded that a significant fraction of the world coastlines exhibit a non-proportional response, prominently under severe SLR scenarios (typically +2 m and beyond), with some regions being above proportional and others being below proportional. We simulated two more severe SLR scenarios (+1.5 m and +2 m), as well as one moderate scenario (+0.5 m) to gain insight into this question over the GBM. The same modelling strategy as for the +1 m SLR simulation was followed for these sensitivity experiments, with SLR imposed at the southern open boundary of the model, with 15 days of spin-up and 14 months long simulation. The simulations were similarly subjected to harmonic analysis. We considered the evolution of M2 tidal constituent, as it dominates the tidal signal. Fig. 7 illustrates the results
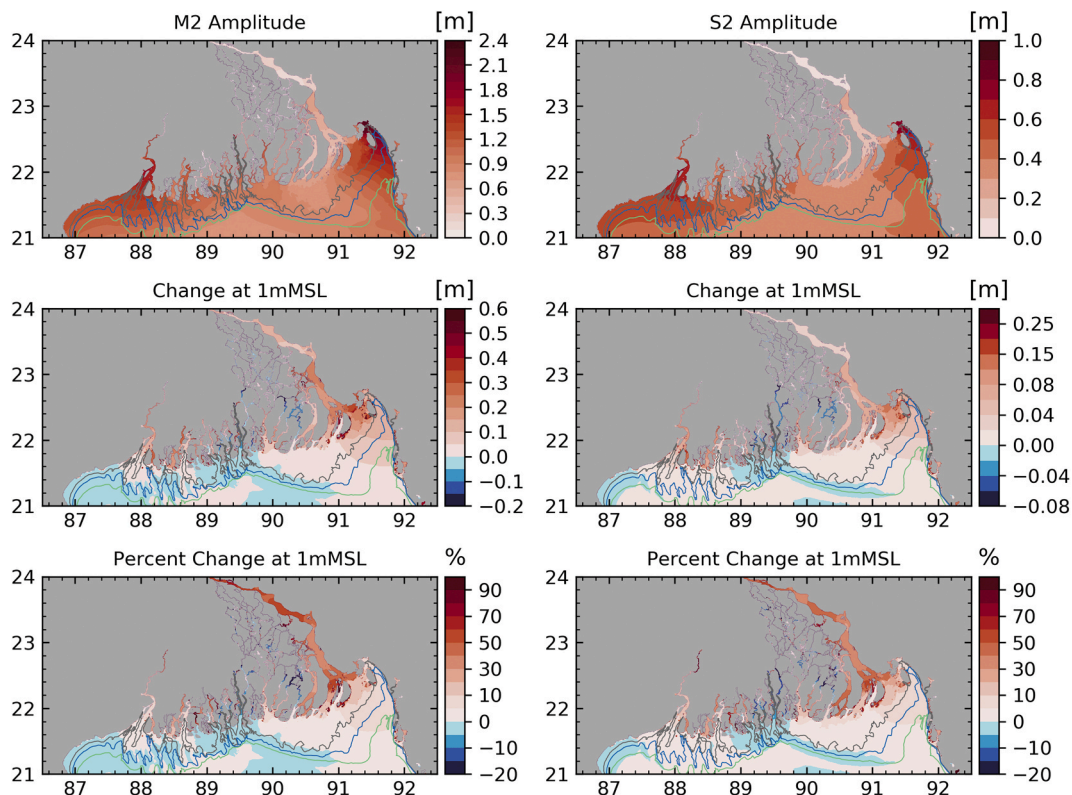

Fig. 5. Amplitude in the reference simulation and difference between the amplitude with +1 m SLR and reference simulations of M2 tidal constituent (left) and for S2 tidal constituent (right). The bottom row shows the difference between the two simulations, expressed in percentage of the amplitudes in the reference simulation.

for three stations located in the eastern part of the GBM, spanning the region of increased tidal range under SLR. Hiron Point is located in the western part of this sub-region as already mentioned in Section 2, Charchanga is located in the central part of this sub-region at the mouth of Meghna, and Chittagong is located in the eastern part (Fig. 1). It is seen that this sub-region shows distinct behaviours from one place to another. The amplitude of M2 appears above-proportional in Charchanga, at the mouth of Meghna, throughout the range of scenarios we tested. While the +0.5 m SLR scenario yields a +1.7 cm amplitude increase (about +2%), the four-fold +2 m SLR scenario shows a +17 cm amplitude increase (20%, or ten-fold the rate of the +0.5 m scenario). In Hiron Point, the change in tidal range shows a non-linear decreasing behaviour, at a similar rate but of opposite sign of Charchanga. In Chittagong, at the eastern edge of the delta, the response in tidal range increase appears roughly proportional, over the whole range of scenarios we tested.

5. Tidal range evolution along the estuaries

As we have seen, the dominant changes in tidal range induced by SLR over the GBM delta, whether positive or negative, are located inside the estuaries. In this section, we examine closely the response predicted by the model in three estuaries, two exhibiting an amplification (Hooghly and Meghna-Brahmaputra-Ganges) and one exhibiting a dampening (Pussur) of tidal range. Fig. 8 presents the profiles of tidal range extracted along the three estuaries, for the present conditions as well as for the various SLR scenarios we tested, from +0.5 m to +2.0 m. For convenience, the tidal range has been normalized by its value at the mouth of the estuary for all cases.

For the Meghna-Brahmaputra-Ganges (Fig. 8b), in present conditions, one can see a decay of the tidal range over the first 50 km of the estuary, with a minimal value amounting to 70% of the value at the mouth, located 50 km upstream of the mouth. Then further upstream the range raises mildly up to 90% at 160 km upstream of the mouth. This location corresponds to the choke point of Chandpur, where the width of the channel abruptly decreases from 6 km to 1 km. There the tidal range collapses sharply. Beyond this choke point, further upstream, the tidal range remains around 30% over more than 100 km. The decreasing-then-increasing profile seen in the downstream part is expected in this kind of long estuary (Dronkers 1964; Du et al., 2018). All SLR scenarios we tested show a similar profile to the present one, though with an upward shift, all along the estuary. The upward shift appears fairly similar for the first three scenarios (+0.5 m, +1.0 m and +1.5 m), with about 10% of excess tidal range for each 0.5 m step of SLR over the lower part (downstream of Chandpur bottleneck) and about 5% of excess tidal range again for each 0.5 m step, upstream of the bottleneck. When considering the most extreme scenarios though (+1.5 m and +2.0 m), the upward shift of tidal range is more modest, around 2% for each 0.5 m step of SLR, from 130 km to 300 km from the mouth. This non-proportionality of the response echoes to the behaviour noted at Hiron Point coastal station (Section 4).

In Hooghly estuary (Fig. 8f), in present conditions we observe a steep increase of tidal range from the mouth up to 60 km upstream, with values 25% higher there than the tidal range at the mouth. Further upstream (60 km–110 km) the tidal range decreases, but remains superior to the value at the mouth. Upstream of 110 km, the tidal range increases again. Just like for Meghna-Brahmaputra-Ganges, the SLR scenarios show a similar profile to the present-day profile for all cases, with an upward shift. The shift also appears quite proportional to the value of SLR we considered from +0.5 m to +1.5 m, with an additional 5% of tidal range per 0.5 m SLR step. From +1.5 m to +2.0 m SLR, we also note a reduction of the tidal range increase, with values at +2.0 m exceeding the values at +1.5 m by 2%. For this estuary as well, which is notably shorter than the Meghna-Brahmaputra-Ganges, such a profile of
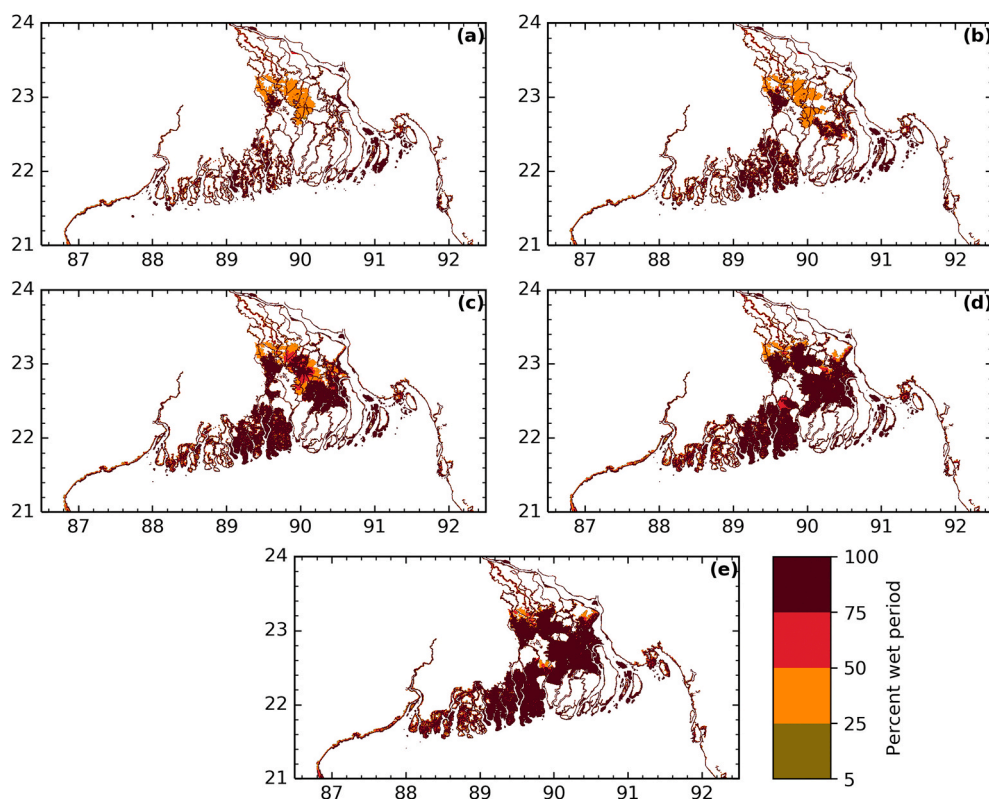

Fig. 6. Map of the frequency of inundation over the model domain, for the reference simulation (a) as well as for the various SLR scenarios we simulated, from +0.5 m (b) to +2 m (e) with 0.5 m stepping. For the sake of readability, we did not shade the already permanent water bodies. (For interpretation of the references to color in this figure legend, the reader is referred to the Web version of this article.)
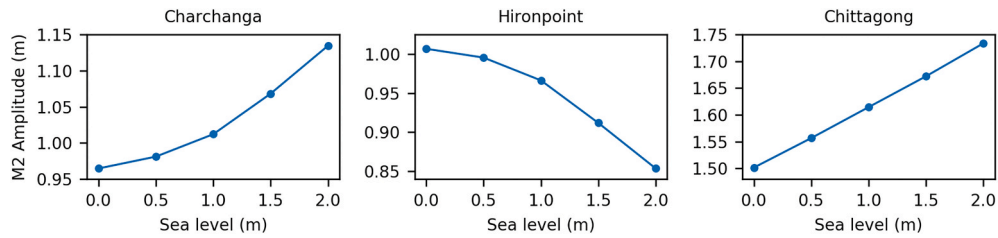
Fig. 7. M2 amplitude modelled at the location of Charchanga (left), Hiron Point (centre) and Chittagong (right), as a function of the magnitude of SLR we imposed in our model, from 0 m (reference simulation) to +2.0 m (most extreme scenario).

consistently higher tidal range inside the estuary compared to the mouth is also consistent with the theoretical cases of Dronkers (1964) or Du et al. (2018). This can be explained by the length of the Hooghly that is closer to its resonant length (amounting to one-fourth of the tidal wavelength), compared to the Meghna-Brahmaputra-Ganges. Indeed, these estuaries have comparable bathymetry (around 10 m throughout, Fig. 8), which results in similar tidal wavelength (180 km for the Meghna-Brahmaputra-Ganges and 140 km for the Hooghly for the semi-diurnal constituents; not shown). For these estuaries, the resonant length thus amounts to about 35–45 km.

For the Pussur estuary (Fig. 8d), the profiles markedly differ from the other two. For present conditions first, we can see a regular increase of tidal range throughout the estuary, up to values 60% above the amplitude of the mouth, 100 km upstream of it. This consistent increase is also

in line with the past studies (e.g. Du et al., 2018) being an estuary closer to resonance compared to the two others. Indeed, the semi-diurnal tidal wavelength amounts to 160 km there, yielding a resonant length of 40 km. What is also completely different from the other two estuaries, expectedly, is the decrease of tidal range in all future SLR scenarios, that we had already seen in the +1 m SLR scenario (Section 4). Each 0.5 m step of SLR yields a decrease of 2%–10% of tidal range when considering the region located 60 km upstream of the mouth. The decrease is larger for the upper steps of SLR (from +1.5 m to +2.0 m). The most extreme scenario we considered, +2.0 m of SLR, yields a profile of tidal range that remains close to the range at the mouth throughout the first 60 km, with a moderate increase further upstream up to 25% of the value of the mouth, hereby strongly lowering the effects of estuarine tidal resonance seen in the present conditions.
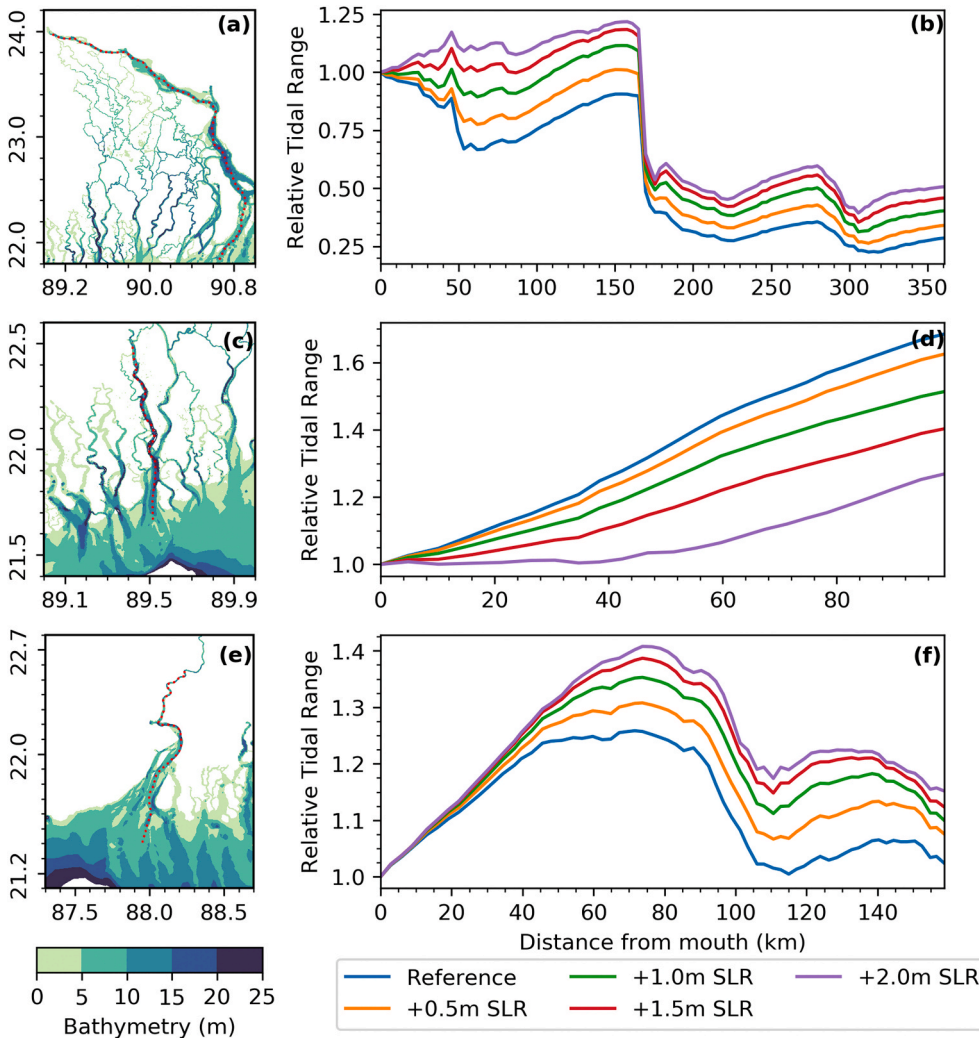

Fig. 8. Bathymetry of the three estuaries considered – Meghna-Ganges-Brahmaputra (a), Pussur (c), and Hooghly (e). Along-estuary profile of tidal range, normalized by the tidal range of the mouth of the Meghna-Ganges-Brahmaputra (b), Pussur (d), and Hooghly (f). Tidal ranges are shown for the reference simulation (blue) as well as for the SLR scenarios we considered (orange for +0.5 m, green for +1.0 m, red for +1.5 m, violet for +2.0 m). The paths of extraction are displayed in red in the maps. (For interpretation of the references to color in this figure legend, the reader is referred to the Web version of this article.)

This contrast between increased tidal range in the Meghna and Hooghly, and decreased tidal range in the Pussur, remains intriguing, as no obvious morphological difference can be seen among these estuaries – all are 3–5 times longer than the resonant length, about 10 m deep throughout, weakly convergent, and probably filled with similar sediment, having similar bottom roughness properties. Fig. 6 already provided a clue about the possible role of new intertidal flats in dissipating the tidal energy in the Pussur, in the future SLR scenarios exceeding +1.0 m. Du et al. (2018) investigated the tidal response to SLR in idealized estuaries, using a numerical model very similar to ours. They considered the cases of solid boundaries along the estuaries, as well as the case of flat floodable banks, that get submerged in SLR scenarios. Our estuaries have geometries that reasonably look like some of their various idealized cases, both in terms of depth and length. Expectedly, it is seen that the behaviour of our three estuaries are in line with theirs, with reduced tidal range for the overflowing Pussur consistent with the response of their "low-lying flat banks" case, and increased tidal range of both Meghna and Hooghly matching their "V-shape channel".

Although our modelling framework, just like that of Du et al. (2018), is dynamically complex (in particular accounting for the non-linearities of the hydrodynamics), and in our case, accounting for the actual geometry of the estuaries at fine scale, it is instructive to interpret our regionally contrasted results in light of the simpler academic cases published in the past studies. The recent review of Talke and Jay (2020) synthesized the idealized framework of constant depth, constant width estuaries, where the tide is subject to linear bottom friction (see their equations 1-2). If we apply this idealized formalism to our three estuaries, we obtain the following. For the Meghna estuary, the semi-diurnal tidal wave (that dominates the tidal signal) has a wavelength of 180 km (not shown). The depth of the estuary lies around 10 m throughout the lower part (south of Chandpur). The length of the estuary, from the mouth to the choke point of Chandpur, amounts to 80 km, that is 40% of the tidal wavelength. Given the Manning coefficient of 0.01 s m$^{-1/3}$ in the estuaries in our model (Krien et al., 2016), this yields a drag coefficient C_d of 5.10^{-4} s^{-1}. The ratio r/ω introduced by Talke and Jay (2020) in their equation (2 d) is the linearized friction coefficient normalized by the angular frequency of the tidal wave. As the amplitude of the tidal current amounts to about 0.6 m s^{-1} (not shown), we get a r/ω ratio of about 0.2. These parameters put the estuary in the category of the long (i.e., much longer than the resonant length) and weakly damped channels. The analytical solution of Talke and Jay (2020) indicates that the tidal amplitude would increase by 4% of the SLR magnitude. As we saw in Fig. 8b, our model predicts a tidal increase amounting to 20% of the SLR in the lower part of the estuary, in qualitative agreement with the theoretical value. If we apply the same theoretical considerations to the Pussur and Hooghly estuaries, we also find that they fall in the same category of long and weakly damped channels, with predicted increase of the tidal range amounting to 10% for Pussur and 4% for Hooghly. Whereas the value for Hooghly is in line with the 8% increase predicted by our model (Fig. 8f), the value for Pussur is not, as our model predicted a *decrease* of the tidal amplitude there, of −15%. This implies that the constant geometry, linear, frictional hydrodynamics of the theoretical model of Talke and Jay (2020) can be invoked to explain the tidal increase for both Meghna and Hooghly estuaries, but it has to be ruled out to explain the tidal decrease in Pussur estuary. One fundamental assumption in the analytical formulation is the constant width, which is certainly not the case in the Pussur at +1 m SLR and beyond, given the massive intertidal flooding seen in Fig. 6. These additional tidal flats will act as a sink of momentum for the tidal wave, which results in an overall decrease of the tidal amplitude. The contrasted behaviour of Meghna and Hooghly estuaries on the one hand, and Pussur estuary on the other hand, appears in line with the findings of Holleman and Stacey (2014). In their modelling of San Francisco Bay, Holleman and Stacey (2014) indeed concluded to a decrease of the tidal amplitude as a response to extended flooding of near-shore diked areas, under future SLR scenarios; however, they modelled an increase of the tidal amplitude if they assumed a rigid shoreline.

6. Discussion

The tidal range in the GBM is seen to evolve significantly under future SLR scenarios, but in diverse ways, depending on the location. The contrasted pattern we obtain, with decreased amplitude in the western and central part of the continental shelf and slope, and increased amplitude in the north-eastern part of it, is qualitatively consistent with the findings of Pickering et al. (2017). We remind that the two forcing strategies are rather different, as they use a global, coarse tidal model, and we use a regional, high-resolution model, with present-day tidal conditions imposed at our open boundary along 11°N. This suggests that the long-term tidal changes to be expected in the Northern Bay of Bengal are prominently generated regionally, in the northern Bay of Bengal itself. This also proves that our southern open boundary, located in the southern Bay of Bengal along 11°N, is far enough from the GBM coast to allow the free development of tidal anomalies in the inner domain of the model, as a response to SLR.

Along the coastline, it is seen that the tidal changes along the open-ocean part of the shore are stronger (positive) both in the eastern and western sides of the delta. This finding is consistent with the seasonal variability of tidal range analysed by Tazkia et al. (2017) using a modelling framework similar to ours. In their study, they concluded that the seasonal changes of M2 amplitude in these two regions were essentially driven by the seasonal variability of the seasonal mean sea level, the wintertime sea level being 0.7 m lower than summertime sea level. They pointed towards the reduced bottom friction as the factor responsible for the stronger tidal amplitude seen at higher water level. As a consequence, one may also point towards the reduced frictional effect of the ocean bottom in the generation of the tidal increase in our SLR scenarios, in these two regions.

In the central part of the delta, in contrast, the widespread negative pattern of tidal trend corresponds closely to the extent of the tidal flooding induced by SLR. This points towards the increased frictional effect of the tide over these additional extended flooded areas as the process responsible for the decay of tidal amplitude.

Inside the estuaries, our model predicts that the tidal changes will be much larger than along the open ocean shoreline in our SLR scenarios, both in terms of absolute magnitude and in terms of percentage of change with respect to current values. Two factors are apparently competing in the frictional behaviour of the estuaries, under SLR conditions – the decreased bottom friction that tends to enhance the tidal amplitude, and the increased sink of dissipation of newly flooded areas that conversely tends to decrease the tidal amplitude. The latter effect dominates the evolution of the dynamical balance in the south-central part of the GBM delta. In contrast, over the rest of the delta, the former factor takes over. In the south-eastern part of the delta in particular, the ubiquitous dikes protecting the polderized land act as rigid boundaries, across the range of SLR scenarios we considered, resulting in a strong tidal amplification there. Thus, the tide appears as an aggravating factor of SLR over both the western and eastern parts of the GBM delta. In contrast, tide stands as a mitigating factor in the south-central delta. In both cases, we make it clear that future studies aiming towards an assessment of the effects of SLR over the GBM delta and associated vulnerability may not leave apart the intricate relationship between tides and SLR. Under a +1 m SLR scenario, the aggravating effect of tidal range exceeds 0.3 m in the Hooghly estuary around 22.5°N, where the city of Kolkata is located. This mechanically implies that the tide will enhance by about 15% of the SLR existing in the ocean, in terms of high-tide water level there. Keeping in mind the socio-economic assets already present in this megacity with 15-million inhabitants (expected to exceed 33 millions by 2050 according to Hoornweg and Pope 2017), the aggravating effect we report in the present study is worth considering in the design of future adaptation policies. The tide will induce a similar aggravation throughout the lower

Meghna, with expectedly similar relevance with regards to the local vulnerability. In contrast, the negative trends seen in the tide in the southern and central parts of the delta, associated with prominent tidal flooding across the area in future scenarios, will act as a mitigating factor of SLR. In some places of the inner delta, this mitigation can reach −0.3 m of tidal range, or −0.15 m of high tide water level, amounting to −15% of the +1.0 m SLR we considered. This amount is considerable, in a context where each centimetre will matter in the evolution of the flooding hazard, and associated vulnerability and risk. This points towards managed re-alignment (Esteves 2014) as an engineering policy that deserves consideration, in the geographical context of the Bengal delta.

Although the water level extremes are expected to respond in a non-linear way to the superimposition of surges and altered tides in future SLR scenarios, is has to be expected that the increased tidal range will increase the probability of tidal and storm surge flooding in this future scenarios, compared to a situation where one would solely consider the SLR process (Idier et al., 2019). Similarly, the seasonal pluvial and compound flooding can be aggravated in the delta due to an amplified tide, particularly during a synchronized peak of the Ganges and Brahmaputra rivers as seen during 1988 and 1998 monsoon food (Mirza 2002).

One limitation of our study resides in our assumption of fixed topography in our future scenarios. It is hard to project what will be the policy implemented in the course of the 21st century over the Bengal delta, in terms of coastal defences. But this policy will certainly have a significant effect on the projections reported here. We also did not account for the vertical land motions nor morphodynamic changes expected to take place over the GBM delta. Although they are not expected to be negligible at centennial timescales, the lack of consistent, synoptic knowledge of the spatial pattern of these vertical motions, precluding a thorough analysis at present, will call for a revisit of our conclusions once such estimates become available.

7. Conclusions

In this study we explore the impact of sea level rise on the tidal properties along the shoreline and estuaries of Bengal delta. From an updated long-term observed timeseries we confirmed that the sea-level along Bengal coast is increasing at a rate of 4 mm/year. We also show that the tidal range can increase at a faster rate compared to the mean sea level. From a set of comprehensive modelling exercises using a high-resolution tidal model we show that there is a large, and regionally-dependent response in tidal properties to future sea level rise scenarios. Regionally the tidal range increases with increase in sea level over the south-western and south-eastern part of the delta. This amplification can significantly aggravate the tidal flooding over these densely populated embanked regions. The tidal amplification is particularly strong along the upstream parts of the esturaries in these two regions. In contrast, over the central part of the delta with extended mangrove area, our model suggests a decrease in tidal range. Being free from man-made embankments, this area experiences extended inland inundation which induces a tidal decay through dissipation. The results presented here shows the presence of a strong regionally-dependent non-linear relationship between sea level rise and tidal properties. We conclude that tidal modulation is a significant factor that needs to be accounted for in the ananlysis of future hydrodynamics, flooding hazard assessment, as well as in delta management policies.

Declaration of competing interest

The authors declare that they have no known competing financial interests or personal relationships that could have appeared to influence the work reported in this paper.

References

Allain, D.J., 2016. TUGOm Tidal Toolbox (ftp://ftp.legos.obs-mip.fr/pub/ecola/tools/ttb.pdf).

Auerbach, L.W., Goodbred, S.L., Mondal, D.R., Wilson, C.A., Ahmed, K.R., Roy, K., Steckler, M.S., Small, C., Gilligan, J.M., Ackerly, B.A., 2015. Flood risk of natural and embanked landscapes on the ganges–brahmaputra tidal delta plain. Nat. Clim. Change 5 (2), 153–157. https://doi.org/10.1038/nclimate2472.

Bamber, J.L., Oppenheimer, M., Kopp, R.E., Aspinall, W.P., Cooke, R.M., 2019. Ice sheet contributions to future sea-level rise from structured expert judgment. Proc. Natl. Acad. Sci. Unit. States Am. 116 (23), 11195–11200. https://doi.org/10.1073/pnas.1817205116.

Becker, M., Papa, F., Karpytchev, M., Delebecque, C., Krien, Y., Khan, J.U., Ballu, V., et al., 2020. Water level changes, subsidence, and sea level rise in the ganges–brahmaputra–meghna delta. Proc. Natl. Acad. Sci. Unit. States Am. https://doi.org/10.1073/pnas.1912921117. January, 201912921.

Benshila, R., Durand, F., Masson, S., Bourdalle-Badie, R., de Boyer Montégut, C., Papa, F., Madec, G., 2014. The upper Bay of Bengal salinity structure in a high-resolution model. Ocean Model. 74, 36–52. https://doi.org/10.1016/j.ocemod.2013.12.001.

Bertin, X., Li, K., Roland, A., Zhang, Y.L., Breilh, J.F., Chaumillon, E., 2014. A modeling-based analysis of the flooding associated with xynthia, central Bay of biscay. Coast. Eng. 94, 80–89. https://doi.org/10.1016/j.coastaleng.2014.08.013. December.

Bomer, E.J., Wilson, C.A., Hale, R.P., Hossain, A.N.M., Rahman, F.M.A., 2020. Surface elevation and sedimentation dynamics in the ganges-brahmaputra tidal delta plain, Bangladesh: evidence for mangrove adaptation to human-induced tidal amplification. Catena 187. https://doi.org/10.1016/j.catena.2019.104312 (April): 104312.

Carrère, L., Lyard, F., Cancet, M., Guillot, A., Roblou, L., 2013. Fes 2012: a new global tidal model taking advantage of nearly 20 Years of altimetry. In: 20 Years of Progress in Radar Altimetry, vol. 710.

Chowdhury, M.A.M., Al Rahim, M., 2012. A proposal on new scheduling of turbine discharge at kaptai hydro-electric power plant to avoid the wastage of water due to overflow in the dam. In: 2012 7th International Conference on Electrical and Computer Engineering. IEEE, pp. 758–762.

Church, J.A., Clark, P.U., Cazenave, A., Gregory, J.M., Jevrejeva, S., Levermann, A., Merrifield, M.A., et al., 2013. sea level change. In: Climate Change 2013: the Physical Science Basis. Contribution of Working Group I to the Fifth Assessment Report of the Intergovernmental Panel on Climate Change. Cambridge University Press, pp. 1137–1216.

Dangendorf, S., Marcos, M., Wöppelmann, G., Conrad, C.P., Frederikse, T., Riva, R., 2017. Reassessment of 20th century global mean sea level rise. Proc. Natl. Acad. Sci. Unit. States Am. 114 (23), 5946–5951. https://doi.org/10.1073/pnas.1616007114.

De Dominicis, M., Wolf, J., Jevrejeva, S., Zheng, P., Hu, Z., 2020. Future interactions between sea level rise, tides and storm surges in the world's largest urban area. Geophys. Res. Lett. 47 https://doi.org/10.1029/2020GL087002 e2020GL087002.

Dronkers, J.J., 1964. Tidal Computations in Rivers and Coastal Waters.

Du, J., Shen, J., Zhang, Y.J., Ye, F., Liu, Z., Wang, Z., Wang, Y.P., Yu, X., Sisson, M., Wang, H.V., 2018. Tidal response to sea-level rise in different types of estuaries: the importance of length, bathymetry, and geometry. Geophys. Res. Lett. 45 (1), 227–235. https://doi.org/10.1002/2017gl075963.

Egbert, G.D., Erofeeva, S.Y., 2002. Efficient inverse modeling of barotropic ocean tides. J. Atmos. Ocean. Technol. 19 (2), 183–204.

Esteves, L.S., 2014. Managed Realignment: A Viable Long-Term Coastal Management Strategy? SpringerBriefs in Environmental Science. Springer Netherlands, Dordrecht. https://doi.org/10.1007/978-94-017-9029-1.

Feng, X., Feng, H., Li, H., Zhang, F., Feng, W., Zhang, W., Yuan, J., 2019. Tidal responses to future sea level trends on the yellow sea shelf. J. Geophys. Res.: Oceans 124 (11), 7285–7306. https://doi.org/10.1029/2019JC015150.

Flather, R.A., 1987. A tidal model of the northeast pacific. Atmos.-Ocean 25 (1), 22–45. https://doi.org/10.1080/07055900.1987.9649262.

Goodbred, S.L., Kuehl, S.A., 1999. Holocene and modern sediment budgets for the Ganges-Brahmaputra river System: evidence for highstand dispersal to flood-plain, shelf, and deep-sea depocenters. Geology 27 (6). https://doi.org/10.1130/0091-7613(1999)027<0559:hamsbf>2.3.co;2, 559.

Haigh, I.D., Pickering, M.D., Green, J.A.M., Arbic, B.K., Arns, A., Dangendorf, S., Hill, D., et al., 2019. The tides they are A-changin': a comprehensive review of past and future non-astronomical changes in tides, their driving mechanisms and future implications. Rev. Geophys. https://doi.org/10.1029/2018RG000636.

Hipel, K.W., McLeod, A.I., 1994. Time Series Modelling of Water Resources and Environmental Systems. Elsevier.

Hirsch, R.M., Slack, J.R., Smith, R.A., 1982. Techniques of trend analysis for monthly water quality data. Water Resour. Res. 18 (1), 107–121. https://doi.org/10.1029/wr018i001p00107.

Holleman, R.C., Stacey, M.T., 2014. Coupling of sea level rise, tidal amplification, and inundation. J. Phys. Oceanogr. 44 (5), 1439–1455. https://doi.org/10.1175/JPO-D-13-0214.1.

Hoornweg, D., Pope, K., 2017. Population predictions for the world's largest cities in the 21st century. Environ. Urbanization 29 (1), 195–216.

Idier, D., Bertin, X., Thompson, P., Pickering, M.D., 2019. Interactions between mean sea level, tide, surge, waves and flooding: mechanisms and contributions to sea level variations at the coast. Surv. Geophys. 40 (6), 1603–1630. https://doi.org/10.1007/s10712-019-09549-5.

Idier, D., Paris, F., Le Cozannet, G., Boulahya, F., Dumas, F., 2017. sea-level rise impacts on the tides of the European shelf. Continent. Shelf Res. 137, 56–71. https://doi.org/10.1016/j.csr.2017.01.007. April.

Kendall, M.G., 1975. Rank Correlation Measures. Charles Griffin, London, 202: 15.

Krien, Y., Karpytchev, M., Ballu, V., Becker, M., Grall, C., Goodbred, S., Calmant, S., Shum, C.K., Khan, Z., 2019. Present-day subsidence in the ganges-brahmaputra-meghna delta: eastern amplification of the holocene sediment loading contribution. Geophys. Res. Lett. 46 (19), 10764–10772. https://doi.org/10.1029/2019gl083601.

Krien, Y., Mayet, C., Testut, L., Durand, F., Tazkia, A.R., Islam, A.K.M.S., Gopalakrishna, V.V., et al., 2016. Improved bathymetric dataset and tidal model for the northern Bay of bengal. Mar. Geodes. 39 (6), 422–438. https://doi.org/10.1080/01490419.2016.1227405.

Krien, Y., Testut, L., Islam, A.K.M.S., Bertin, X., Durand, F., Mayet, C., Tazkia, A.R., et al., 2017a. Towards improved storm surge models in the northern Bay of bengal. Continent. Shelf Res. 135, 58–73. https://doi.org/10.1016/j.csr.2017.01.014. March.

Krien, Y., Dudon, B., Roger, J., Arnaud, G., Zahibo, N., 2017b. Assessing storm surge hazard and impact of sea level rise in the lesser antilles case study of Martinique. Nat. Hazards Earth Syst. Sci. 17 (9), 1559–1571. https://doi.org/10.5194/nhess-17-1559-2017.

Mann, H.B., 1945. Nonparametric tests against trend. Econometrica 13 (3). https://doi.org/10.2307/1907187, 245.

McCreary, J.P., Han, W., Shankar, D., Shetye, S.R., 1996. Dynamics of the east India coastal current, 2. Numerical solutions. J. Geophys. Res. 101, 13993–14010.

Mirza, M.Q., 2002. Global warming and changes in the probability of occurrence of floods in Bangladesh and implications. Global Environ. Change 12 (2), 127–138. https://doi.org/10.1016/S0959-3780(02)00002-X.

Mukhopadhyay, S.K., Biswas, H., De, T.K., Jana, T.K., 2006. Fluxes of nutrients from the tropical river hooghly at the land–ocean boundary of sundarbans, NE coast of Bay of bengal, India. J. Mar. Syst. 62 (1–2), 9–21. https://doi.org/10.1016/j.jmarsys.2006.03.004.

Neumann, B., Vafeidis, A.T., Zimmermann, J., Nicholls, R.J., 2015. Future coastal population growth and exposure to sea-level rise and coastal flooding - a global assessment. Edited by Lalit Kumar PloS One 10 (3). https://doi.org/10.1371/journal.pone.0118571. e0118571.

Oppenheimer, M., Glavovic, B., Hinkel, J., van de Wal, R., Magnan, A.K., Abd-Elgawad, A., Cai, R., et al., 2019. sea level rise and implications for low lying islands, coasts and communities. In: IPCC Special Report on the Ocean and Cryosphere in a Changing Climate.

Pethick, J., Orford, J.D., 2013. Rapid rise in effective sea-level in southwest Bangladesh: its causes and contemporary rates. Global Planet. Change 111, 237–245. https://doi.org/10.1016/j.gloplacha.2013.09.019. December.

Pickering, M.D., Horsburgh, K.J., Blundell, J.R., Hirschi, J.J.M., Nicholls, R.J., Verlaan, M., Wells, N.C., 2017. The impact of future sea-level rise on the global tides. Continent. Shelf Res. 142, 50–68. https://doi.org/10.1016/j.csr.2017.02.004. June.

Rahman, M., Dustegir, M., Karim, R., Haque, A., Nicholls, R.J., Darby, S.E., Nakagawa, H., Hossain, M., Dunn, F.E., Akter, M., 2018. Recent sediment flux to the ganges-brahmaputra-meghna delta System. Sci. Total Environ. 643, 1054–1064. https://doi.org/10.1016/j.scitotenv.2018.06.147. December.

Rahman, S., Islam, A.K.M.S., Saha, P., Tazkia, A.R., Krien, Y., Durand, F., Testut, L., Islam, G.M.T., Bala, S.K., 2019. Projected changes of inundation of cyclonic storms in the ganges–brahmaputra–meghna delta of Bangladesh due to SLR by 2100. Journal of Earth System Science 128 (6). https://doi.org/10.1007/s12040-019-1184-8.

Ray, R.D., 1999. A Global Ocean Tide Model from TOPEX/POSEIDON Altimetry: GOT99.2. National Aeronautics and Space Administration, Goddard Space Flight Center.

Ray, R.D., 2013. Precise comparisons of bottom-pressure and altimetric ocean tides. J. Geophys. Res.: Oceans 118 (9), 4570–4584.

Sen, P.K., 1968. Estimates of the regression coefficient based on Kendall tau. J. Am. Stat. Assoc. 63 (324), 1379–1389. https://doi.org/10.1080/01621459.1968.10480934.

Shankar, D., McCreary, J.P., Han, W., Shetye, S.R., 1996. Dynamics of the East India Coastal Current 1. Analytic solutions forced by interior Ekman pumping and local alongshore winds. J. Geophys. Res. 101 (13) https://doi.org/10.1029/96JC00559, 991.

Sindhu, B., Unnikrishnan, A.S., 2013. Characteristics of tides in the Bay of bengal. Mar. Geodes. 36 (4), 377–407. https://doi.org/10.1080/01490419.2013.781088.

Sweet, W.V., Kopp, R.E., Weaver, C.P., Obeysekera, J., Horton, R.M., Thieler, E.R., Zervas, C., 2017. Global and Regional Sea Level Rise Scenarios for the United States.

Talke, S.A., Jay, D.A., 2020. Changing tides: the role of natural and anthropogenic factors. Annual Review of Marine Science 12 (1), 121–151. https://doi.org/10.1146/annurev-marine-010419-010727.

Tazkia, A.R., Krien, Y., Durand, F., Testut, L., Islam, A.K.M.S., Papa, F., Bertin, X., 2017. Seasonal modulation of M2 tide in the northern Bay of bengal. Continent. Shelf Res. 137, 154–162. https://doi.org/10.1016/j.csr.2016.12.008. April.

Tessler, Z.D., Vorosmarty, C.J., Grossberg, M., Gladkova, I., Aizenman, H., Syvitski, J.P.M., Foufoula-Georgiou, E., 2015. Profiling risk and sustainability in coastal deltas of the world. Science 349 (6248), 638–643. https://doi.org/10.1126/science.aab3574.

Woodworth, P.L., 2010. A survey of recent changes in the main components of the ocean tide. Continent. Shelf Res. 30 (15), 1680–1691. https://doi.org/10.1016/j.csr.2010.07.002.

Woodworth, P.L., 2012. A note on the nodal tide in sea level records. J. Coast Res. 280, 316–323. https://doi.org/10.2112/JCOASTRES-D-11A-00023.1. March.

World Bank, 2005. Project Performance Assessment Report - Coastal Embankment Rehabilitation Project. World Bank, Washington, 31565. https://ieg.worldbankgroup.org/sites/default/files/Data/reports/ppar_31565.pdf.

Zhang, Y., Baptista, A.M., 2008. SELFE: a semi-implicit eulerian–Lagrangian finite-element model for cross-scale ocean circulation. Ocean Model. 21 (3–4), 71–96. https://doi.org/10.1016/j.ocemod.2007.11.005.

Zhang, Y.J., Ye, F., Stanev, E.V., Grashorn, S., 2016. Seamless cross-scale modeling with SCHISM. Ocean Model. 102, 64–81. https://doi.org/10.1016/j.ocemod.2016.05.002. June.